The Link between the North Atlantic Oscillation and Arctic Sea Ice Export through Fram Strait

THOMAS JUNG AND MICHAEL HILMER

Institut für Meereskunde an der Universität Kiel, Kiel, Germany

(Manuscript received 16 October 2000, in final form 11 April 2001)

ABSTRACT

Recently, Hilmer and Jung have shown that the wintertime link between the North Atlantic oscillation (NAO) and the sea ice export through Fram Strait changed from zero correlation (1958–77) to about 0.7 (1978–97) during the last four decades. In the current study, the authors focus on the question of how the two phenomena are linked in a long-term context during wintertime (December–March). This is done on a statistical basis using data from a century-scale control integration of the coupled general circulation model ECHAM4–OPYC3 along with historical sea level pressure data for the period 1908–97.

From the results of this study there is less indication that a significant link on interannual and decadal timescales between the NAO and the sea ice export through Fram Strait is a characteristic property of the climate system—at least under present-day climate conditions. This missing link can be explained by a vanishing net impact of the NAO on sea ice thickness as well as sea ice drift near Fram Strait and thus the sea ice volume export through Fram Strait. It is argued that the spatial pattern of interannual NAO variability as observed during the last two decades of the twentieth century is unusual and so is the high correlation between the NAO and Arctic sea ice export for the period 1978–97.

1. Introduction

The North Atlantic oscillation (NAO)—a phenomenon that is well known for many decades—is the dominant mode of North Atlantic atmospheric variability and describes the simultaneous strengthening and weakening of the Azores high and Icelandic low (e.g., Defant 1924; Walker 1924; Cayan 1992; Hurrell 1995). Recently, the link between the NAO and Arctic sea ice export through Fram Strait during wintertime has attracted increasing scientific interest (e.g., Kwok and Rothrock 1999; Dickson et al. 2000; Hilmer and Jung 2000). This is (among other reasons) because sea ice export through Fram Strait provides a variable source of surface freshwater for the northern North Atlantic Ocean (e.g., Aagaard and Carmack 1989; Hilmer et al. 1998; Vinje et al. 1998), which may subsequently alter the convective activity in the high-latitude North Atlantic and therefore the strength of the North Atlantic thermohaline circulation (e.g., Mauritzen and Häkkinen 1997).

Whereas some modeling studies (Tremblay et al. 1997; Häkkinen and Geiger 2000) suggest a negative but rather weak connection between the NAO and Arctic sea ice export through Fram Strait, recent observational work indicates a high positive correlation between both phenomena during the winters of the last two decades. Using an 18-yr record of passive microwave satellite data, Kwok and Rothrock (1999) found a positive correlation (correlation coefficient $r = 0.66$) between the NAO and the remotely sensed ice area flux through Fram Strait during wintertime (December–March: DJFM). This finding is in agreement with the results by Dickson et al. (2000), who report a positive correlation between the NAO index and the parameterized[1] sea ice export through Fram Strait during wintertime ($r = 0.77$ from 1976 to 1996). It is worth stressing that both estimates do not account for interannual sea ice thickness variability in Fram Strait. In summary, the results by Kwok and Rothrock (1999) and Dickson et al. (2000) support the following conclusion (WCRP 1998):

> . . . the NAO appears to exert a significant control on the export of ice and freshwater from the Arctic to the open Atlantic, ...

The link between the NAO and Arctic sea ice export through Fram Strait during wintertime was revisited by Hilmer and Jung (2000, hereinafter HJ00) using a hindcast simulation of a dynamic–thermodynamic sea ice model that was solely forced by daily near-surface wind speed and air temperature fields taken from the National Centers for Environmental Prediction–National Center

Corresponding author address: Dr. Thomas Jung, ECMWF, Shinfield Park, Reading RG2 9AX, United Kingdom.
E-mail: thomas.jung@ecmwf.int

[1] SLP gradient along Fram Strait times a fixed value for ice thickness in Fram Strait.

for Atmospheric Research (NCEP–NCAR) reanalysis project (Kalnay et al. 1996) for the period 1958–97. In agreement with the observational studies by Kwok and Rothrock (1999) and Dickson et al. (2000), HJ00 found a significant positive correlation ($r = 0.70$) between the observed NAO index and the modeled Arctic sea ice volume export through Fram Strait for winters from 1978 to 1997. However, HJ00 also showed that a significant link between the two time series was missing ($r = 0.06$) during the period 1958–77. Other groups independently described similar changes in the link between the two time series (e.g., Arfeuille et al. 2000). As pointed out by HJ00, this secular change in the link between the NAO and Arctic sea ice export through Fram Strait during the last four decades can be traced back to secular changes in the longitudinal position of the NAO's centers of interannual variability (HJ00, their Fig. 4).

To summarize, from previous studies described above it remains unclear whether a link or a missing link between the NAO and the export of Arctic sea ice through Fram Strait during wintertime is a characteristic property of the climate system. It is the objective of this study to shed further light onto this question. For this purpose, however, it is neither possible to use observational sea ice data nor is it possible to use realistic hindcast simulations of a sea ice model (realistic forcing data). This is because the reliability of data over the Arctic decreases considerably because of sampling problems as we go back in time. Therefore, we follow another strategy making use of two alternative datasets. First, the link is directly studied using a century-scale integration of a state-of-the-art coupled atmosphere–ocean–sea ice general circulation model (GCM) under present-day climate conditions. Second, observed secular changes of the spatial pattern of interannual NAO variability during the twentieth century are studied using historical sea level pressure (SLP) data. From these spatial patterns the link between the two phenomena during the twentieth century is inferred assuming that interannual sea ice export variability through Fram Strait is primarily governed by geostrophic wind anomalies.

The paper is organized as follows. The data used throughout this study are described in section 2. Then, in section 3, the coupled GCM's fidelity to simulated Arctic sea ice properties is assessed. In section 4 the results from this coupled GCM integration are used to analyze long-term characteristics as well as time-dependent aspects of the link between the NAO and Arctic sea ice export through Fram Strait. Then, in section 5, these findings are discussed in the context of secular changes of *observed* interannual NAO variability during the period 1908–97. A discussion and our conclusions are given in sections 6 and 7, respectively.

2. Models and data

a. Coupled GCM: ECHAM4/OPYC3

To study the link between the NAO and Arctic ice volume flux through Fram Strait we analyze a century-scale (300 yr) integration of the European Centre for Medium-Range Weather Forecasts (ECMWF)–Hamburg (ECHAM4)–Ocean Isopycnal Model (OPYC3) coupled atmosphere–ocean–sea ice model under present-day climate conditions (i.e., concentrations of greenhouse gases are fixed to the observed 1990 values; Roeckner et al. 1996, 1999). The atmospheric component, ECHAM4, is the fourth generation of a hierarchy of models that was developed at the Max Planck Institute in Hamburg, Germany, from the former ECMWF model. ECHAM4 has a horizontal resolution of T42 (approximately 2.8° by 2.8°) and 19 hybrid levels in the vertical. OPYC3 is a three-component model including an isopycnal interior ocean, a mixed layer component, and a dynamic–thermodynamic sea ice model that represents internal stresses by a viscous–plastic rheology (Oberhuber 1993). The horizontal resolution poleward of 38° is identical to that of the atmospheric model. The meridional resolution increases toward the equator (0.5°) to properly resolve the equatorial waveguide. Vertically, 11 layers were used. Zonal and meridional ice flux components are formulated as prognostic variables. An annual mean flux correction scheme has been applied to air–sea heat and freshwater fluxes over the oceans. In the presence of sea ice the flux correction is only applied to surface heat fluxes. Note that no flux correction has been applied to wind stress fields. Further details are given elsewhere (Roeckner et al. 1996, 1999; Bacher et al. 1998).

b. Kiel sea ice model (KSIM) integration

Climatological sea ice properties of the coupled GCM are compared with results from a realistic hindcast simulation of the Kiel sea ice model, an optimized dynamic–thermodynamic sea ice model with viscous–plastic rheology and 1° × 1° horizontal resolution (Harder et al. 1998; Hilmer et al. 1998; Kreyscher et al. 2000, and references therein). KSIM was forced with daily fields of near-surface winds and air temperatures taken from the NCEP–NCAR reanalysis project (Kalnay et al. 1996) over the period 1958–97. Oceanic heat fluxes into an oceanic mixed layer with fixed depth were prescribed as climatological annual cycles; oceanic near-surface currents were prescribed as annual means. Both oceanic forcing fields were derived from a coupled ocean–sea ice model integration of Hibler and Zhang (1994). Further details about the "KSIM integration" used in this study are given elsewhere (Hilmer et al. 1998; Hilmer 2001).

c. Sea level pressure fields: 1908–97

Observed interannual variability of the NAO during the twentieth century is studied using gridded SLP data (5° × 5°) over the Northern Hemisphere north of 15°N and for the period 1908–97 [updated version from Trenberth and Paolino (1980)]. Errors and discontinuities are

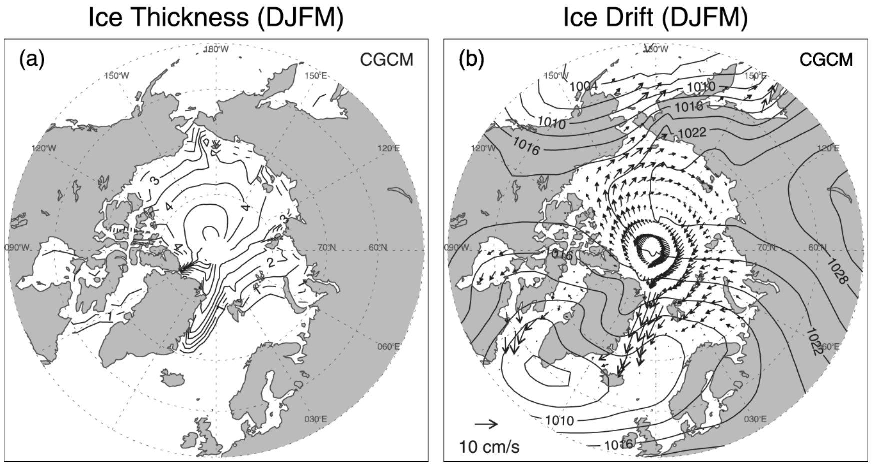

FIG. 1. Long-term mean winter-averaged (DJFM) (a) sea ice thickness (m) as well as (b) sea ice drift vectors and sea level pressure (hPa) over the Arctic as simulated by the coupled GCM (300 yr). In (b), every second vector in longitudinal direction has been omitted. A reference vector for sea ice drift (10 cm s^{-1}) is given.

reported for this dataset by Trenberth and Paolino (1980). These occur primarily before 1922, particularly over parts of Asia. Problems also exist north of 70°N due to sparse sampling and in low latitudes where the signal-to-noise ratio is relatively low.

d. *The NAO index*

Following the methodology for the observations (e.g., Rogers 1984; Hurrell 1995) the NAO index is defined as the difference between *normalized* SLP of the Azores high and the Icelandic low. The normalization (i.e., removing the mean and dividing by the standard deviation) has been done separately for each month. Last, winter averages (DJFM) were formed using the monthly NAO indices.

For the coupled GCM, variability of the Azores high (Icelandic low) is described by SLP averaged over the region 40°–42.5°N and 10°–15°W (65°–67.5°N and 17.5°–20°W). In this coupled GCM these regions show the strongest teleconnectivity (Christoph et al. 2000) and represent the centers of action of the first EOF of North Atlantic SLP anomalies (not shown).

The *observed* NAO index (see section 5) is based on monthly station data taken from the Azores and Iceland.

e. *Sea ice export through Fram Strait*

The ice volume flux (IVF) through Fram Strait is calculated for a zonal section in the coupled GCM connecting the northeastern tip of Greenland with Spitsbergen, Norway, according to

$$\mathrm{IVF} = \int_{\Gamma} \upsilon(r)h(r)\,dr, \qquad (1)$$

where r now denotes the position along the section Γ, $\upsilon(r)$ is the ice drift component perpendicular to this section, and $h(r)$ is the ice thickness along Γ. (We use r instead of x to highlight that generally other choices than a zonal section for Γ are possible.) Furthermore, the southward drift speed (SDS) of sea ice through Fram Strait and the ice thickness in Fram Strait (hereinafter h) are determined by averaging over all grid points along Γ. Because of the usage of different grids in the coupled GCM and KSIM, the sections Γ differ slightly between the two models (Γ as used by KSIM is located slightly farther northward in comparison with the coupled model).

3. Model assessment

In this section the performance of the coupled GCM to simulate the mean state and variability around the mean state of the Arctic sea ice cover during wintertime is assessed. The results from the coupled GCM are compared with results from the realistic hindcast simulation of KSIM over the period 1958–97. The latter integration serves as ''observational truth.'' On large spatial scales this is reasonable since the results from the KSIM integration agree well with what is known from the observations (HJ00; Kreyscher 1998; Hilmer 2001; Kreyscher et al. 2000).

a. *Modeled mean state*

Mean sea ice thickness and sea ice drift fields in the Arctic during wintertime as simulated by the coupled GCM are depicted in Fig. 1, those from the KSIM integration are shown in Fig. 2. Although the coupled GCM appears to realistically simulate the gross features of mean Arctic sea ice properties, some differences com-

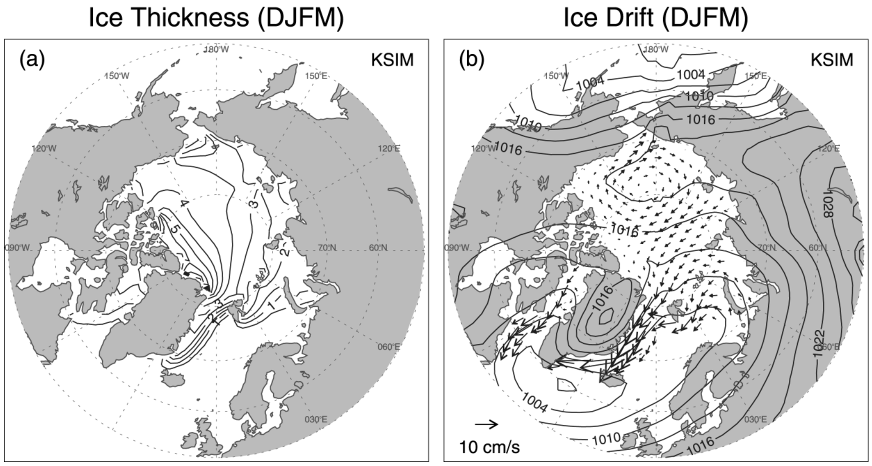

FIG. 2. As in Fig. 1, but for the realistic hindcast simulation using the KSIM. Details about this integration are given elsewhere (Hilmer et al. 1998; Hilmer 2001). In (b), only every fourth vector is shown. Sea level pressure data are from the NCEP–NCAR reanalysis (Kalnay et al. 1996).

pared to the KSIM integration are evident. The anticyclonic Beaufort gyre as simulated by the coupled GCM, for instance, is biased toward the North Pole in comparison with observations (Colony and Thorndike 1984) and KSIM. This leads to thinner ice in the Beaufort Sea region but to thicker ice in the Kara Sea in comparison with KSIM. Moreover, differences between the two model integrations are also noteworthy for sea ice thickness north of Greenland and upstream of as well as within Fram Strait (Table 1). Whereas, because of its model grid structure, the maximum sea ice thickness in the coupled GCM is located directly over the North Pole, the KSIM integration reveals largest mean values north of Greenland and in the north of the Canadian archipelago, which is more realistic in comparison with the observations (Bourke and McLaren 1992, their Fig. 4b).

Long-term mean ice thickness (h) and SDS in Fram Strait from both model integrations are summarized in Table 1 along with modeled IVF. IVF and SDS are in good agreement, whereas the coupled GCM simulates a much smaller h in Fram Strait than KSIM. This difference is partly attributable to the sharper longitudinal ice thickness gradient within Fram Strait of the GCM, which in turn is caused by differences in the mean ice drift patterns. It may surprise that the mean IVF agrees quite well although the mean sea ice thickness differs considerably. (The length of the sections Γ is very similar.) To explain this item it is necessary to break down the mean IVF into different components. Both sea ice quantities can be decomposed using $x = [x] + x^*$ and $x = \overline{x} + x'$, where x denotes either ice thickness or SDS, $[x]$ is the average along Γ, x^* denotes deviations from $[x]$, the overbar stands for the temporal mean, and the prime denotes temporal anomalies. Applying this breakdown to Eq. (1) and temporal averaging leads to

$$\overline{\mathrm{IVF}} = [\overline{v}][\overline{h}]\Gamma + \overline{[v'][h']}\Gamma + \int \overline{v}^*\overline{h}^*\, dx + \int \overline{v'^*h'^*}\, dx. \qquad (2)$$

The left-hand side of Eq. (2) is given in Table 1 and amounts to 0.086 Sv (1 Sv $= 10^6$ m^3 s^{-1}) for the coupled model. Whereas contributions from the second and fourth term on the right-hand side are negligible for the coupled GCM, the contribution from the first (third) term amounts to 0.064 Sv (0.025 Sv). For KSIM the mean IVF is almost solely governed by the first term on the right-hand side of Eq. (2). These differences explain why the mean IVF in the coupled GCM and KSIM agrees relatively well although the mean sea ice thickness differs considerably.

It is worth noting that any direct comparison of mean IVF between the two models is difficult to carry out. This is because large north–south sea ice thickness gradients occur in the long-term mean near Fram Strait, thus, leading to a strong sensitivity of the mean IVF to small changes in the latitudinal position used to define the Fram Strait section Γ.

When comparing sea ice climatologies from the coupled GCM with observational datasets or other model

TABLE 1. Mean and std dev for winter averages (DJFM) of the IVF through Fram Strait as well as SDS and ice thickness h in Fram Strait as simulated by the coupled GCM ECHAM4–OPYC3 (300 yr) and the KSIM over the period 1958–97.

	ECHAM4–OPYC3			KSIM		
	IVF (Sv)	SDS (cm s^{-1})	h (m)	IVF (Sv)	SDS (cm s^{-1})	h (m)
Avg	0.086	7.49	1.34	0.116	7.39	3.60
Std dev	0.030	2.16	0.35	0.033	1.96	0.38

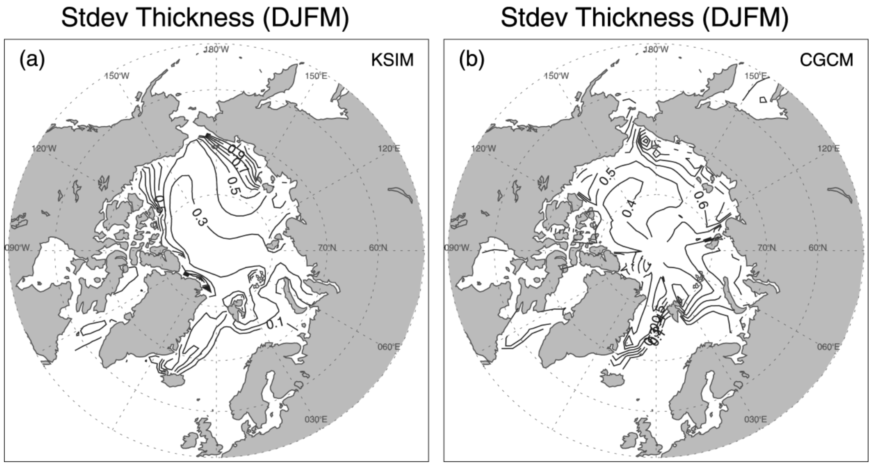

FIG. 3. Interannual std dev (m) of simulated wintertime sea ice thickness: (a) KSIM and (b) coupled GCM.

integrations it has to be kept in mind that an annual-mean flux correction scheme has been applied to surface heat fluxes in the presence of sea ice in the coupled GCM integration. Thus, some agreement between simulated and observed annual-mean Arctic sea ice cover may simply be due to flux correction. Note, however, that no flux corrections were applied to wind stress fields.

b. *Modeled variability*

The standard deviation of winter-averaged sea ice quantities in Fram Strait is also shown in Table 1 for the two models. Obviously, variability of sea ice quantities in Fram Strait during wintertime as simulated by the coupled GCM is in good agreement with those obtained from the KSIM integration. This similarity is not very sensitive to small changes in the latitudinal position of Fram Strait [Γ in Eq. (1)] because in both models

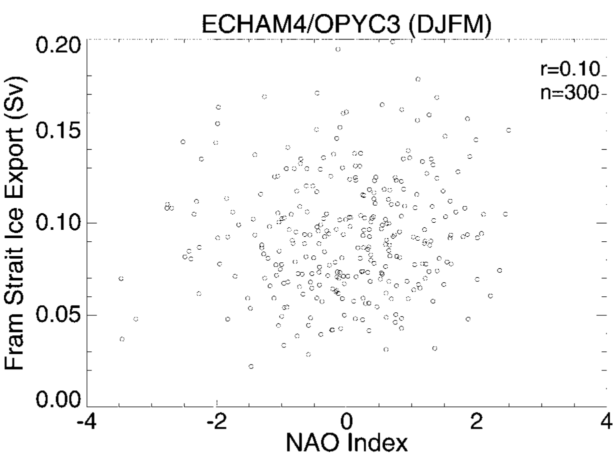

FIG. 4. Ice export through Fram Strait (Sv) vs NAO index during wintertime (DJFM) as simulated by the coupled GCM (n = 300 yr). The correlation coefficient r = 0.10.

gradients of sea ice thickness and southward drift speed variability are relatively small near Fram Strait (not shown).

For the whole Arctic, the spatial patterns of the interannual ice thickness variability (Fig. 3) agree quite well between both models, despite some differences between the corresponding long-term mean fields. Both patterns exhibit largest amplitudes of the wintertime standard deviation in the East Siberian and Beaufort Seas but relatively small variability within the central Arctic. Although a comparison with observational data is not possible, this structure agrees well with results of other modeling studies (e.g. Flato 1995; Arfeuille et al. 2000).

To summarize, differences between the two models show up primarily for the long-term mean state. The agreement between the two models is much better in terms of climate variability. Therefore we feel confident that the coupled GCM integration is useful to shed further light onto the link between the NAO and the sea ice export out of the Arctic through Fram Strait.

4. Modeled link

a. *Long-term characteristics*

A scatterplot of the IVF and the NAO index as simulated by the coupled GCM for 300 subsequent winters is depicted in Fig. 4. The linear correlation coefficient $r = 0.10$; that is, in the coupled GCM the amount of variance of IVF that can be linearly explained by the NAO is negligibly small. Moreover, neither SDS of sea ice nor sea ice thickness in Fram Strait are significantly correlated with the NAO index ($r = -0.03$ and $r = -0.06$, respectively). Last, visual inspection of Fig. 4 does not indicate any noteworthy nonlinear relationship between the two time series.

To take into account the possibility that the link between the ice volume export through Fram Strait and

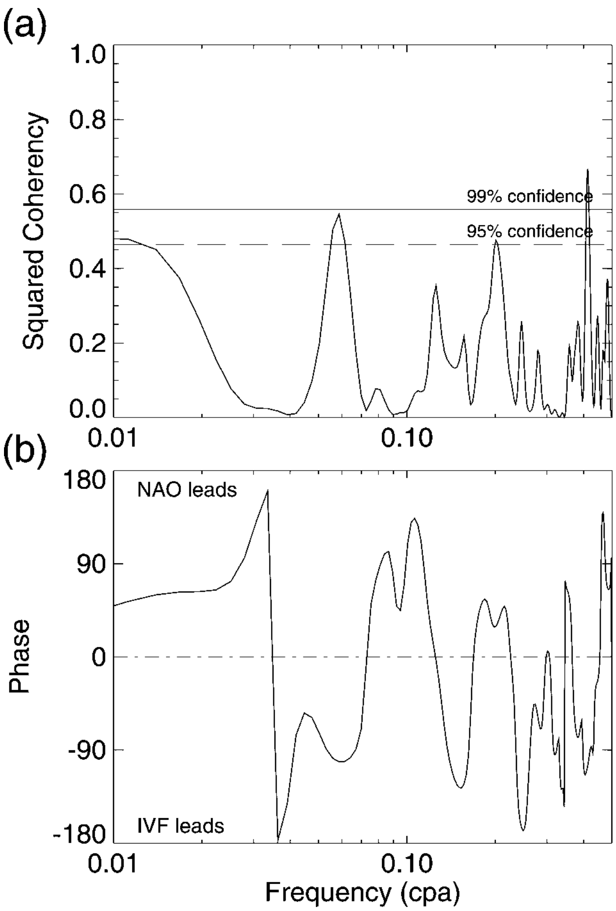

FIG. 5. (a) Squared coherency and (b) phase spectrum for winter averages (DJFM) of the NAO index and IVF through Fram Strait from the coupled GCM (300 yr). The NAO leads for positive phases. A Tukey window with a maximum lag of 60 yr was used for smoothing (12.4 degrees of freedom). The 95% (dashed) and 99% (dash–dotted) confidence levels for nonzero coherency are displayed in (a).

the NAO index is timescale dependent and/or not directly in phase, the link between the two time series was studied in the spectral domain by applying cross-spectral analysis (Fig. 5). Except for a few narrow peaks the estimated squared coherency is relatively low and the estimated phase appears to vary more or less randomly over the frequency range under study (about 2–100 yr). On secular timescales (about 100 yr), for instance, the NAO leads IVF, whereas IVF leads the NAO in a narrow frequency band around 17 yr. While we cannot not definitely exclude that these *locally* significant squared coherencies are due to some physical processes, we note that significant peaks for squared coherency in specific frequency ranges can also occur just by chance for two statistically independent time series. Moreover, none of the two time series reveals pronounced power in the frequency bands of significant squared coherency (not shown). Similar arguments hold for the narrow peaks on interannual timescales (Fig. 5). Thus, it is clear that the ‘‘coupling’’ between the two

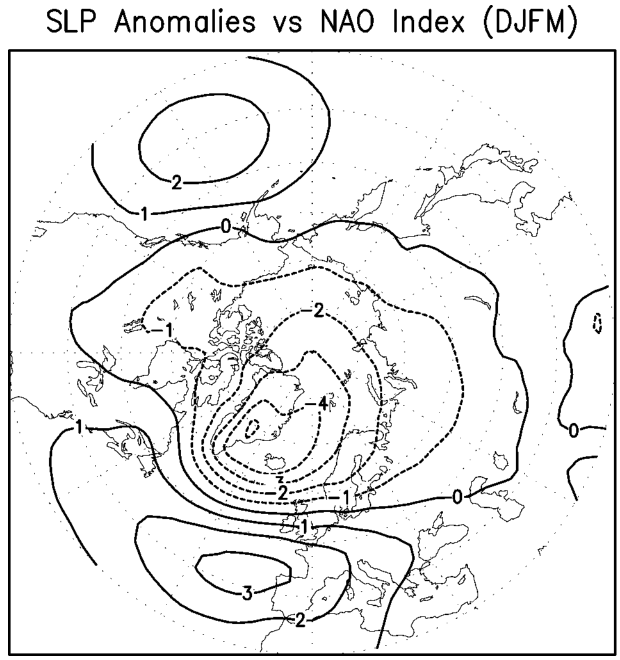

FIG. 6. SLP anomalies (hPa) that are associated with the NAO index in the coupled GCM during wintertime (DJFM). SLP anomalies were linearly regressed onto the normalized NAO index.

time series for narrow frequency bands—even if not purely accidental—does not contribute noteworthily to the total variance of the two time series. To summarize, there is no evidence for a noteworthy wintertime link between the NAO and Arctic sea ice export through Fram Strait in the coupled GCM. This holds for different timescales and phases.

In order to clarify why the NAO exerts no significant control on the Arctic sea ice export through Fram Strait in the coupled GCM, the spatial pattern of the NAO was estimated by regressing SLP anomalies onto the normalized NAO index (Fig. 6). In the North Atlantic region and over the Arctic the spatial pattern of the NAO as simulated by the coupled GCM resembles the observed one during the period 1958–77 (HJ00, their Fig. 4a), that is, during a period when a link between the observed NAO index and the modeled ice volume export through Fram Strait was missing. As argued by HJ00, the vanishing correlation between the two time series can be explained by the fact that the NAO pattern shows no anomalous meridional geostrophic wind components near Fram Strait that might have affected the SDS of sea ice in Fram Strait and thus the sea ice volume export through Fram Strait.

That this argument also holds for the coupled GCM becomes evident from Fig. 7, which shows the Arctic sea ice response during wintertime to a forcing by the NAO (i.e., sea ice thickness and sea ice drift anomalies that were linearly associated with the NAO index). High-NAO winters, for instance, are accompanied by anomalously low ice thicknesses around Spitsbergen,

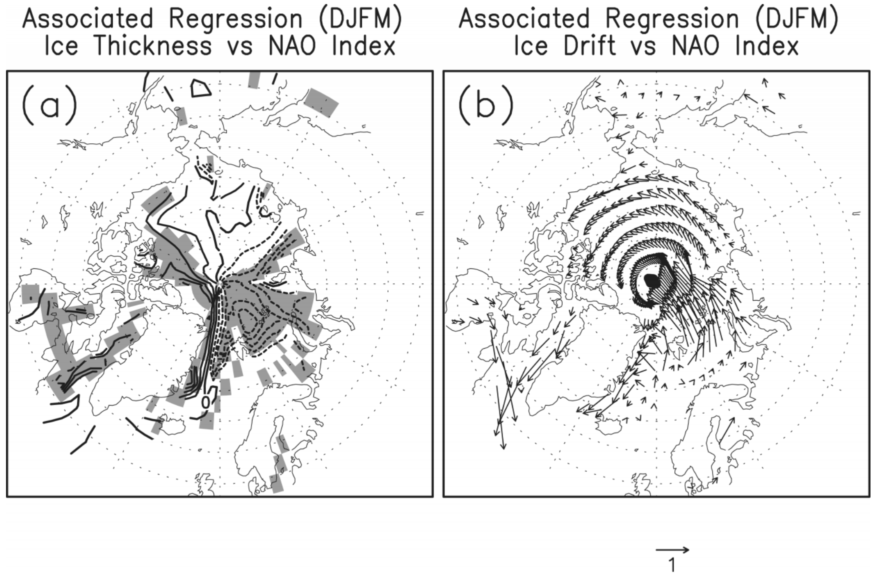

FIG. 7. As in Fig. 6, but for (a) ice thickness anomalies (m) and (b) anomalous zonal and meridional ice drift components. Contour interval in (a) is 0.03 m, and shading denotes statistical significance (at 95% confidence). A reference vector (1 cm s^{-1}) is given in (b). For clarity, every second vector in longitudinal direction was omitted.

Norway, and Franz-Josef-Land, Russia, and above-normal ice thicknesses around the northeastern coast of Greenland, north of Greenland, and the Canadian archipelago, as well as in the Labrador Sea/Baffin Bay region. These anomalies, whose magnitudes amount to about 0.1 m near the centers of action, can be explained by the combined effect of NAO-related near-surface temperature (thermodynamic forcing) and near-surface wind speed (dynamic forcing) anomalies. Note that such a NAO-related dipole is also well known for observed sea ice concentration anomalies (e.g., Fang and Wallace 1994; Deser et al. 2000). The percentage of sea ice thickness variance that can locally be explained by the NAO in the Arctic, however, does not exceed 10% in the coupled GCM. In Fram Strait NAO-related positive and negative ice thickness anomalies cancel each other. This explains the relatively weak correlation between the NAO index and total sea ice thickness in Fram Strait. Sea ice drift anomalies that are associated with the NAO index (Fig. 7b) agree with what can be expected from a direct local wind stress forcing by the NAO (Fig. 6). Others than for long-term means (Fig. 1) anomalous sea ice drift vectors are almost parallel to the anomalous NAO-related isobars. Although NAO-related meridional sea ice drift anomalies are present in Fram Strait, the net sea ice drift in Fram Strait vanishes because of opposite anomalies at the western and eastern side of Fram Strait. Looking at Fig. 7 it becomes evident that the NAO forces thicker sea ice out of, and thinner sea ice into, the Arctic. This holds for high- and low-NAO winters and therefore has no influence on the linear relationship between the NAO and Arctic sea ice export. However, since the percentage of sea ice thickness and sea ice drift variance in Fram Strait that can linearly be explained by the NAO is very small, this effect is negligible. [Note that this is consistent with the vanishing effect from the fourth term on the right-hand side of Eq. (2).] In summary, in this coupled GCM the influence of the NAO on local sea ice properties in Fram Strait is such that the NAO cannot exert a significant control on the ice volume export through Fram Strait.

The anomalous SLP pattern that is associated with high ice volume export events through Fram Strait in the coupled GCM is depicted in Fig. 8 (''Fram pattern''). This pattern is very similar to that obtained if the IVF time series from KSIM is used instead (HJ00, their Fig. 4c). The center of action of the Fram pattern is located over the Kara Sea giving rise to anomalous meridional (geostrophic) wind components near Fram Strait. Note that this SLP pattern shows no pronounced SLP anomalies near Iceland and the Azores, thus indirectly supporting the notion that in this coupled GCM it is not the NAO that is forcing sea ice export anomalies through Fram Strait.

b. *Time dependence*

Once the long-term characteristics of the link between the NAO and Arctic ice export as simulated by the coupled GCM are described, its time dependence is then investigated. The cross-correlation function (19-yr running window) of the NAO index and the ice export time series is shown in Fig. 9 along with the low-pass-filtered (19-yr running mean) NAO index. Out of the 282 overlapping chunks (19-yr length) the highest cross correlation between the NAO index and the sea ice export

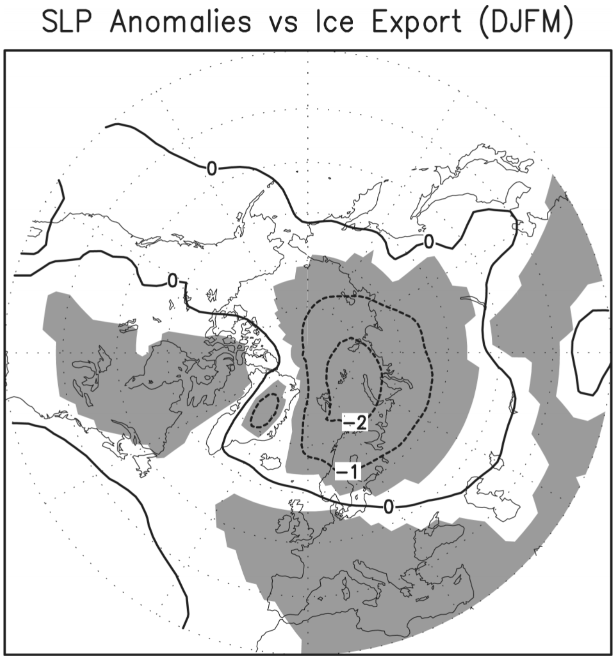

FIG. 8. Same as in Fig. 6, but for the SLP anomalies and the normalized ice volume export through Fram Strait. Statistically significant slope parameters (at 95% confidence) are shaded.

does not exceed $r = 0.58$. Note, that a correlation of $r = 0.70$ was found during the period 1978–97 from the realistic hindcast simulation using KSIM (HJ00) and that the percentage of variance explained by a linear relationship is quadratic in the correlation coefficient. The long-term average of the cross-correlation function is about zero and its standard deviation is $\sigma = 0.25$. Thus, provided that the coupled GCM performs realistically in simulating natural variability of the NAO and Arctic sea ice, the relatively high correlation between the NAO and the ice volume flux through Fram Strait as observed during the last two decades appears to be rather unusual.

A Monte Carlo test was performed in order to investigate how the cross-correlation coefficient is distributed under the null hypothesis that the NAO index and the ice volume export through Fram Strait as simulated by the coupled GCM are realizations of independent first-order autoregressive [AR(1)] processes. AR(1) parameters were estimated from the time series. Then, 10 000 realizations of the null hypothesis, each having a length of 19 yr, were generated; 2.5th and 97.5th percentiles of the estimated cross-correlation coefficients are given by -0.45 and 0.47, respectively. Seven excursions of the cross-correlation function above the 97.5th percentile occur in Fig. 9. Note, however, that on average $0.025 \times 282 \approx 7$ excursions are expected to occur just by chance—even for *independent* estimates (of course, the cross-correlation coefficients in Fig. 9 are *not* independent). The standard deviation of the ensemble of cross correlations amounts to $\sigma =$

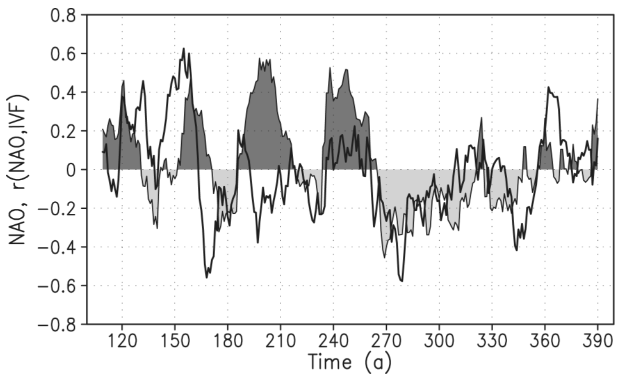

FIG. 9. Interdecadal NAO variability (19-yr running mean, solid) along with the cross-correlation function for the NAO index and ice volume export through Fram Strait (19-yr running window, shaded) for winter-averaged data (DJFM) from the coupled GCM (300-yr control integration). Time is given in model years. The model year 110, for instance, denotes the 19-yr period 101–119.

0.24, which is in close agreement with the estimate obtained from the data ($\sigma = 0.25$, see above).

As noted by HJ00, the observed increase in the covariability between the NAO index and the Arctic sea ice export through Fram Strait during the last four decades came in parallel with the secular increase of the NAO. The correlation between low-frequency variability of the NAO and the cross-correlation function between the two time series (Fig. 9) is rather weak ($r = 0.31$) in the coupled GCM. An additional Monte Carlo test was performed to assess the unusualness of a correlation coefficient of $r = 0.31$ taking into account the strong serial correlation (lag-1 correlation > 0.9) of the time series in Fig. 9. Results from the Monte Carlo test show that 2.5th and 97.5th percentiles are given by $r_{2.5} = -0.77$ and $r_{97.5} = 0.77$, respectively. Hence, there is no statistical evidence that interdecadal changes of the NAO do exert a significant control on the coherence between the NAO and the ice export on interannual timescales—at least in the control integration of the ECHAM4–OPYC3 model.

In summary, the time dependence of the link between the NAO index and the sea ice export through Fram Strait as simulated by the coupled GCM (Fig. 9) is consistent with what is expected from realizations of two independent processes. This conclusion is supported by the results of Ulbrich and Christoph (1999) showing that the spatial pattern of interannual NAO variability remained unchanged during the course of the control integration of the ECHAM4–OPYC3 model (resembling those shown in Fig. 6).

5. Changes of interannual NAO variability: 1908–97

The results from the coupled GCM support the conclusion that the link between the NAO and the sea ice export through Fram Strait is rather weak. This suggests that interannual NAO variability as observed during the

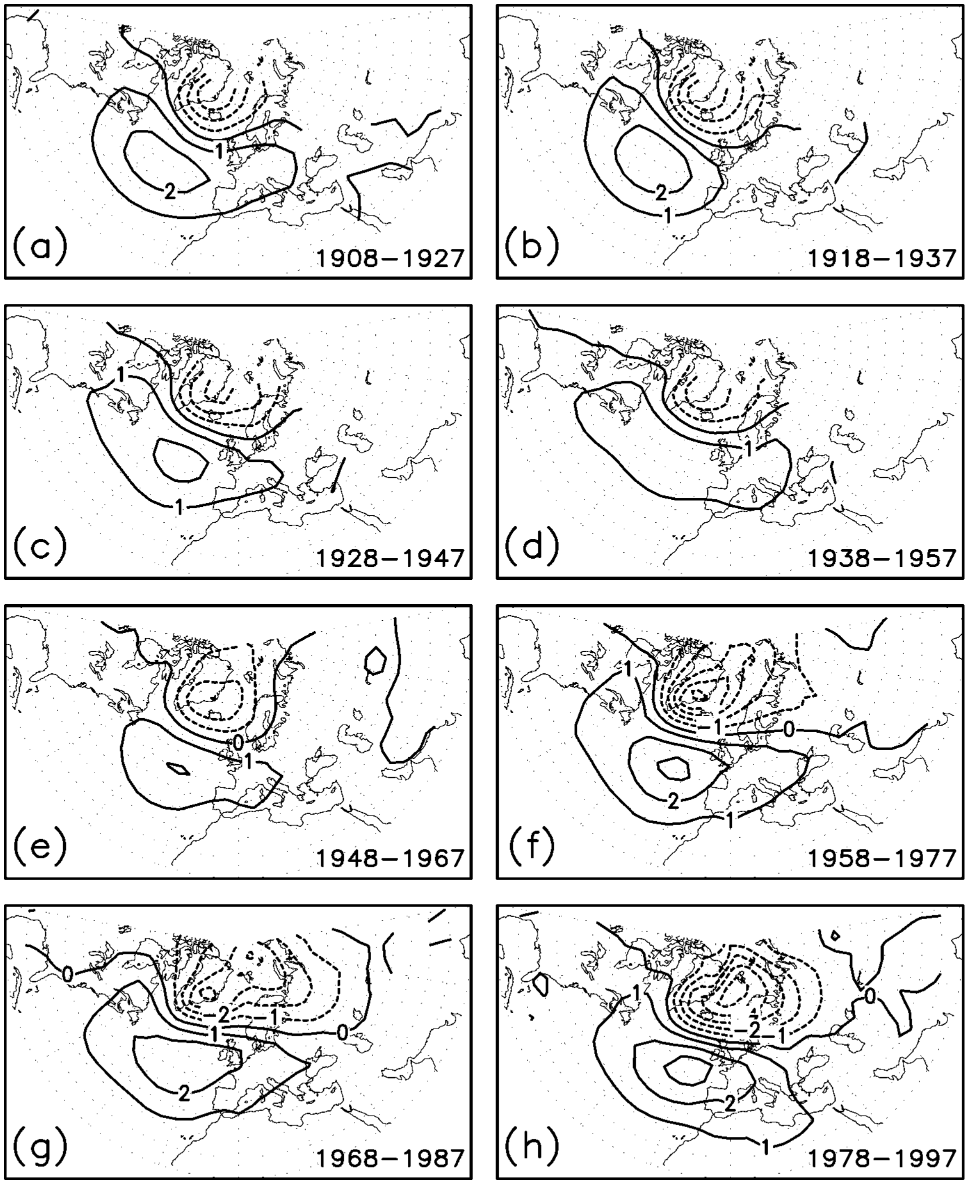

FIG. 10. SLP anomalies (hPa) that are associated with the NAO index during the winters (DJFM): (a) 1908–27, (b) 1918–37, (c) 1928–47, (d) 1938–57, (e) 1948–67, (f) 1958–77, (g) 1968–87, and (h) 1978–97. SLP anomalies were linearly regressed onto the NAO index. Note that no normalization was applied to the NAO index for each of the periods. Linear trends were removed beforehand in (a)–(h). Slope parameters are only shown for those grid points with nonmissing data during the respective period.

period 1958–78 (a period when a significant link between the two time series was missing; HJ00, their Fig. 4a) is more representative in the long-term context. To test this hypothesis—as far as possible—for the observations, we studied how the spatial structure of interannual NAO variability has changed during the period 1908–97. Keeping in mind that modeled time series of the sea ice export through Fram Strait are not available before the middle of the twentieth century, our argument is necessarily qualitative in nature. That is, we infer the strength of the link between the two time series only from meridional wind speed anomalies near Fram Strait inferred from the location of the northern center of interannual NAO variability.

Spatial patterns of observed interannual NAO variability for overlapping 20-yr periods during the twentieth century (1908–97) are depicted in Fig. 10. The patterns were obtained by regressing SLP anomalies onto the NAO index for each of the 20-yr periods. To allow for a direct comparison between different periods, no additional normalization was applied to the NAO index for each of the periods. In the northern North

Atlantic the spatial structures of all the six patterns of interannual NAO variability for the period 1908–77 are very much similar (Figs. 10a–f) as can be inferred from the center of action of the anomalous Icelandic low that is located over eastern Greenland. Note that this spatial structure resembles those from the control integration of the coupled GCM (Fig. 6). In agreement with the study by HJ00 (HJ00 used SLP data from the NCEP–NCAR reanalysis), pronounced changes of interannual NAO variability took place around the late 1970s.[2] Thus, the spatial structure of observed interannual NAO variability during the last two decades (1978–97) is rather unusual in a longer-term context (1908–97) and we conclude—by inference—that a significant link between the NAO and the sea ice export through Fram Strait was missing during the period 1908–77.

While (presumably) not important for the conclusions of this study, we note for completeness that the magnitudes of the NAO-related SLP anomalies underwent secular changes too. This can partly be traced back to sampling variability due to the finite length of the time series. The role of contributions from secular changes in the number of SLP observations per winter entering the analyses, and thus the uncertainty of winter averages, is more difficult to assess. Such an undersampling definitely has consequences for the magnitude of the slope parameters obtained by linear regression; however, we presume this problem to be of minor importance, at least for the spatial structures.

6. Discussion

a. Link between NAO and Arctic sea ice export

While the NAO doubtless exerts a significant control on a variety of different climate parameters in the North Atlantic and Arctic region (e.g., Hurrell and van Loon 1997; Dickson et al. 2000) including sea ice concentrations in the Labrador Sea and the Greenland/Icelandic/Norwegian Seas (e.g., Fang and Wallace 1994; Deser et al. 2000), our study suggests that a significant forcing of Arctic sea ice export through Fram Strait by the NAO during wintertime, as is evident for the last two decades (Kwok and Rothrock 1999; Dickson et al. 2000; HJ00), is rather unusual in a long-term context. One might criticize that our conclusions about the link between the two time series suffer from the fact that no long *observational* time series of the Arctic sea ice export was used. (Continuous observational estimates for the sea ice drift and sea ice thickness in Fram Strait are only available since 1978 and 1990, respectively.) While this is clearly somewhat unsatisfactory, we feel confident that our major conclusions, which are based on modeling results, are realistic. This is because the models appear to simulate key aspects realistically and—most important—the modeled strength of the link between the two time series agrees with what we do expect from our physical reasoning, that is, sea ice export anomalies through Fram Strait are largely driven by anomalous atmospheric flow fields.

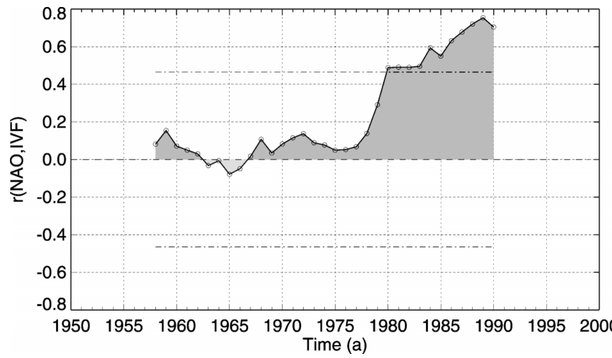

Fig. 11. Running cross-correlation function (19-yr window) between NAO index and simulated ice volume export through Fram Strait for winters (DJFM) from 1949 to 1999. The 95% confidence levels (dashed) indicate correlation coefficients which are significantly different from zero. A two-sided Student's *t* test was applied taking into account both the serial correlation of the whole time series and the window length of 19 yr. For each of the windows linear trends were removed beforehand.

While finalizing this manuscript an extended version of the NECP–NCAR reanalysis became available (1948–99). We used these new forcing data to extend the KSIM integration over the period 1949–99. The year 1948 was excluded from the analysis since it may be inflated by the model's spinup. [Details about this integration are given in Hilmer (2001).] The running cross-correlation function between winter averages of the NAO index and the modeled sea ice export through Fram Strait using a window length of 19 yr is depicted in Fig. 11. The change in the link between the two time series that took place around the late 1970s (HJ00) is clearly evident. Moreover, there is no indication for the existence of a significant link between the two time series during the 1950s—thus, further supporting the conclusions of this study.

While the focus of this study (and previous studies) was on the winter season (DJFM), from an oceanographic point of view sea ice exports through Fram Strait during the other seasons may be of importance too. We have also looked onto the link between the NAO and the sea ice export through Fram Strait during the nonwinter seasons. In the coupled GCM, there is no significant link ($r \approx 0.0$) between the two time series during nonwinter seasons (MAMJ, JJAS, SOND). The KSIM integrations reveals negative but small correlation coefficients between the two times series during the other seasons. Thus, a rather weak link between the NAO and Arctic sea ice export through Fram Strait appears to be characteristic for nonwinter seasons.

[2] As pointed out by HJ00, the fact that the eastward shift of interannual NAO variability during the last four decades is also evident for SLP analyses (Figs. 10f–h) shows that this shift is not an artifact of the reanalysis due to changes in observational practices (e.g., use of satellite data).

b. Changes of interannual NAO variability

As found out by HJ00, recent changes in the link between the NAO and Arctic sea ice export through Fram Strait can be explained by changes in the spatial structure of interannual NAO variability. The eastward shift of the NAO's centers of interannual NAO variability, which appears to be unprecedended during the twentieth century (Fig. 10), led also to pronounced changes in NAO-related interannual variability of the number of deep cyclones, near-surface air temperatures, and net surface heat fluxes in the North Atlantic region (Jung 2000). Thus, it is important to unravel possible causes for the recent shift of interannual NAO variability.

A possible explanation is provided by the study of Ulbrich and Christoph (1999). (A detailed physical mechanism is still missing, however.) They analyzed a control and a scenario integration of the same coupled GCM as is used in the present study (ECHAM4–OPYC3) and found a systematic northeastward shift of the NAO's northern variability center under enhanced greenhouse gas concentrations (after 2020 or so). In the control integration the centers of action were rather fixed. Therefore, one might speculate that the observed recent shift of interannual NAO variability is caused by enhanced greenhouse gas concentrations. To further test this hypothesis, it is important, however, to investigate whether similar changes of interannual NAO variability are evident (i) from control *and* scenario integrations of other coupled GCMs and (ii) from different ensemble integrations of the same coupled GCM. To our knowledge, relatively few studies have dealt so far with possible changes of interannual NAO variability under enhanced greenhouse gas concentrations (e.g., Ulbrich and Christoph 1999; Paeth et al. 1999; Monahan et al. 2000).

Recently, Palmer (1993, 1999) proposed a nonlinear dynamical perspective on climate variability and change. From this perspective an external forcing may primarily appear as a change in the frequency of occurrence of fixed natural modes of atmospheric variability (e.g., NAO), rather than as a change in the location of natural modes. Evidence for the validity of this nonlinear paradigm is presented from observations by Corti et al. (1999) and from a coupled GCM integration by Monahan et al. (2000). On the other hand, the results from Ulbrich and Christoph (1999), HJ00, and this study suggest that the location of the centers of NAO variability can undergo secular changes (although presumably not very frequently under present-day climate conditions). We cannot exclude, however, that changes in the occupation statistics of more than one fixed natural mode of variability led to changes in the location of the NAO. From the above discussion it becomes clear that still some work remains to improve our understanding about (possible low-frequency changes of) the atmospheric attractor, both under present-day climate conditions as well as under enhanced anthropogenic emission scenarios (e.g., enhanced greenhouse gas and sulfate concentrations).

7. Conclusions

The nature of the wintertime link between the NAO and Arctic sea ice export anomalies through Fram Strait is investigated. The results from a century-scale control integration of the coupled atmosphere–ocean–sea ice model ECHAM4–OPYC3 under present-day climate conditions support the following conclusions.

- There is no significant wintertime link ($r \approx 0.0$) between the NAO and the export of Arctic sea ice through Fram Strait (Fig. 4). This holds for variability from interannual to interdecadal timescales (Fig. 5).
- Changes in the ice volume export through Fram Strait are associated with significant SLP anomalies over the Kara Sea (Fig. 8).
- Interdecadal changes in the link on interannual timescales between the two time series (under present-day climate conditions) are consistent with what can be expected for two statistically independent time series.

The spatial NAO pattern as simulated by the coupled GCM (Fig. 6) resembles those found by HJ00 for the period 1958–77 when a significant link between the NAO index and the modeled ice export was missing. The analysis of historical SLP data (1908–97) reveals that this pattern was also characteristic for the first part of the twentieth century (1908–77; Fig. 10). Thus, the following conclusion can be drawn.

- The existence of a significant link between the NAO and the sea ice export out of the Arctic, as found during the last two decades of the twentieth century (Kwok and Rothrock 1999; Dickson et al. 2000) due to an eastward shift of the NAO's centers of interannual variability (HJ00), is rather unusual—at least in the context of natural climate variability.

Acknowledgments. Drs. C. Eden and J. E. Walsh provided valuable comments to previous versions of the manuscript. Drs. E. Ruprecht and P. Lemke supported this study. Drs. E. Roeckner, J. M. Oberhuber, and M. Esch kindly provided data from the control integration of the ECHAM4–OPYC3 model. Author T. Jung benefited from hospitality at Alfred Wegener Institute (AWI) Foundation for Polar and Marine Research, Bremerhaven, Germany. This is a contribution of the Sonderforschungsbereich 460 ''Dynamics of Thermohaline Circulation Variability'' at the University of Kiel (available online at http://www.ifm.uni-kiel.de/general/sfb460-e.html) supported by the German Research Foundation.

REFERENCES

Aagaard, K., and E. C. Carmack, 1989: The role of sea ice and other fresh water in the Arctic circulation. *J. Geophys. Res.*, **94,** 14 485–14 498.

Arfeuille, G., L. A. Mysak, and L.-B. Tremblay, 2000: Simulation of interannual variability of the wind-driven Arctic sea ice cover during 1958–1998. *Climate Dyn.,* **16,** 107–121.

Bacher, A., J. W. Oberhuber, and E. Roeckner, 1998: ENSO dynamics and seasonal cycle in the tropical Pacific as simulated by the ECHAM4/OPYC3 coupled general circulation model. *Climate Dyn.,* **14,** 431–450.

Bourke, R. H., and A. S. McLaren, 1992: Contour mapping of Arctic basin ice draft and roughness parameters. *J. Geophys. Res.,* **97,** 17 715–17 728.

Cayan, D. R., 1992: Latent and sensible heat flux anomalies over the northern oceans: The connection to monthly atmospheric circulation. *J. Climate,* **5,** 354–369.

Christoph, M., U. Ulbrich, J. M. Oberhuber, and E. Roeckner, 2000: The role of ocean dynamics for low-frequency fluctuations of the NAO in a coupled ocean–atmosphere GCM. *J. Climate,* **13,** 2536–2549.

Colony, R., and A. S. Thorndike, 1984: An estimate of the mean field of Arctic sea ice motion. *J. Geophys. Res.,* **89,** 10 623–10 629.

Corti, S., F. Molteni, and T. N. Palmer, 1999: Signature of recent climate change in the frequency of natural atmospheric circulation regimes. *Nature,* **398,** 799–802.

Defant, A., 1924: Die Schwankungen der atmosphärischen Zirkulation über dem Nordatlantischen Ozean im 25-jährigen Zeitraum 1881–1905. *Geogr. Ann.,* **6,** 13–41.

Deser, C., J. E. Walsh, and M. S. Timlin, 2000: Arctic sea ice variability in the context of recent atmospheric circulation trends. *J. Climate,* **13,** 617–633.

Dickson, R. R., and Coauthors, 2000: The Arctic Ocean response to the North Atlantic oscillation. *J. Climate,* **13,** 2671–2696.

Fang, Z., and J. M. Wallace, 1994: Arctic sea ice variability on a timescale of weeks and its relation to atmospheric forcing. *J. Climate,* **7,** 1897–1914.

Flato, G. M., 1995: Spatial and temporal variability of Arctic ice thickness. *Ann. Glaciol.,* **21,** 323–329.

Häkkinen, S., and C. A. Geiger, 2000: Simulated low-frequency modes of circulation in the Arctic Ocean. *J. Geophys. Res.,* **105,** 6549–6564.

Harder, M., P. Lemke, and M. Hilmer, 1998: Simulation of sea ice transport through Fram Strait: Natural variability and sensitivity to forcing. *J. Geophys. Res.,* **103,** 5595–5606.

Hibler, W. D., and J. Zhang, 1994: On the effect of circulation on Arctic ice-margin variations. *The Polar Oceans and their Role in Shaping the Global Environment, Geophys. Monogr.,* No. 85, Amer. Geophys. Union, 383–397.

Hilmer, M., 2001: A model study of Arctic sea ice variability. Berichte aus dem Institut für Meereskunde Kiel No. 320, Institut für Meereskunde an der Universität Kiel, Kiel, Germany, 157 pp.

——, and T. Jung, 2000: Evidence for a recent change in the link between the North Atlantic oscillation and Arctic sea ice export. *Geophys. Res. Lett.,* **27,** 989–992.

——, M. Harder, and P. Lemke, 1998: Sea ice transport: A highly variable link between Arctic and North Atlantic. *Geophys. Res. Lett.,* **25,** 3359–3362.

Hurrell, J. W., 1995: Decadal trends in the North Atlantic oscillation: Regional temperatures and precipitation. *Science,* **269,** 676–679.

——, and H. van Loon, 1997: Decadal variations in climate associated with the North Atlantic oscillation. *Climatic Change,* **36,** 301–326.

Jung, T., 2000: The North Atlantic oscillation: Variability and interactions with the North Atlantic Ocean and Arctic sea ice. Berichte aus dem Institut für Meereskunde Kiel No. 315, Institut für Meereskunde an der Universität Kiel, Kiel, Germany, 117 pp.

Kalnay, E., and Coauthors, 1996: The NCEP/NCAR 40-Year Reanalysis Project. *Bull. Amer. Meteor. Soc.,* **77,** 437–471.

Kreyscher, M., 1998: Dynamics of Arctic sea ice—Validation of different rheology schemes for the use in climate models. Berichte zur Polarforschung No. 291, Alfred-Wegener-Institut, Bremerhaven, Germany, 116 pp.

——, M. Harder, P. Lemke, and G. M. Flato, 2000: Results of the sea ice model intercomparison project: Evaluation of sea ice rheology schemes for use in climate simulations. *J. Geophys. Res.,* **105,** 11 299–11 320.

Kwok, R., and D. A. Rothrock, 1999: Variability of Fram Strait ice flux and North Atlantic oscillation. *J. Geophys. Res.,* **104,** 5177–5189.

Mauritzen, C., and S. Häkkinen, 1997: Influence of sea ice on the thermohaline circulation in the Arctic–North Atlantic Ocean. *Geophys. Res. Lett.,* **24,** 3257–3260.

Monahan, A. H., J. C. Fyfe, and G. M. Flato, 2000: A regime view of Northern Hemisphere atmospheric variability and change under global warming. *Geophys. Res. Lett.,* **27,** 1139–1142.

Oberhuber, J. M., 1993: Simulation of the Atlantic circulation with a coupled sea ice–mixed layer–isopycnal general circulation model. Part I: Model description. *J. Phys. Oceanogr.,* **23,** 808–829.

Paeth, H., A. Hense, R. Glowienka-Hense, R. Voss, and U. Cubasch, 1999: The North Atlantic oscillation as an indicator for greenhouse-gas induced regional climate change. *Climate Dyn.,* **15,** 953–960.

Palmer, T. N., 1993: Extended-range atmospheric prediction and the Lorenz model. *Bull. Amer. Meteor. Soc.,* **74,** 49–65.

——, 1999: A nonlinear dynamical perspective on climate prediction. *J. Climate,* **12,** 575–591.

Roeckner, E., J. M. Oberhuber, A. Bacher, M. Christoph, and I. Kirchner, 1996: ENSO variability and atmospheric response in a global coupled atmosphere–ocean GCM. *Climate Dyn.,* **12,** 737–754.

——, L. Bengtsson, J. Feichter, J. Lelieveld, and H. Rhode, 1999: Transient climate change simulations with a coupled atmosphere–ocean GCM including the tropospheric sulfur cycle. *J. Climate,* **12,** 3004–3032.

Rogers, J. C., 1984: The association between the North Atlantic oscillation and the Southern oscillation in the Northern Hemisphere. *Mon. Wea. Rev.,* **112,** 1999–2015.

Tremblay, L.-B., L. A. Mysak, and A. S. Dyke, 1997: Evidence from driftwood records for century-to-millenial scale variations of the high latitude atmospheric circulation during Holocene. *Geophys. Res. Lett.,* **24,** 2027–2030.

Trenberth, K. E., and D. A. Paolino, 1980: The Northern Hemisphere sea-level pressure data set: Trends, errors and discontinuities. *Mon. Wea. Rev.,* **108,** 855–872.

Ulbrich, U., and M. Christoph, 1999: A shift of the NAO and increasing storm track activity over Europe due to anthropogenic greenhouse gas forcing. *Climate Dyn.,* **15,** 551–559.

Vinje, T., N. Nordlund, and A. Kvambekk, 1998: Monitoring ice thickness in Fram Strait. *J. Geophys. Res.,* **103,** 10 437–10 449.

Walker, G. T., 1924: Correlation in seasonal variation of weather, IX. *Mem. Indian Meteor. Dep.,* **24,** 275–332.

WCRP 1998: CLIVAR initial implementation plan. WMO/TD 869, World Climate Research Program Rep. 103, 314 pp.